Sharifian Mazraeh Mollaei, Masoud; Hurshkainen, A.; Kurdjumov, S.; Glybovski, S.; Simovski, Constantin

Decoupling of Two Closely Located Dipole Antennas by a Split-Loop Resonator

Published in:
Radio Science

DOI:
10.1029/2018RS006679

Published: 01/11/2018

Document Version
Publisher's PDF, also known as Version of record

AGU100 ADVANCING EARTH AND SPACE SCIENCE

Radio Science

RESEARCH ARTICLE

10.1029/2018RS006679

Key Points:

- Two very closely resonant dipole antennas are decoupled
- Ultrahigh field MRI is the main application
- Mutual impedance between dipole antenna and Split-Loop Resonator is derived

Correspondence to:
M. Sharifian Mazraeh Mollaei,
Masoud.2.sharifianmazraehmollaei@aalto.fi

Citation:
Sharifian Mazraeh Mollaei, M., Hurshkainen, A., Kurdjumov, S., Glybovski, S., & Simovski, C. (2018). Decoupling of two closely located dipole antennas by a split-loop resonator. *Radio Science*, *53*. https://doi.org/10.1029/2018RS006679

Received 9 JUL 2018
Accepted 18 OCT 2018
Accepted article online 20 OCT 2018

Decoupling of Two Closely Located Dipole Antennas by a Split-Loop Resonator

M. Sharifian Mazraeh Mollaei[1], A. Hurshkainen[2], S. Kurdjumov[2], S. Glybovski[2], and Constantin Simovski[1]

[1]Department of Electronics and Nanoengineering, Aalto University, Espoo, Finland, [2]Department of Electrical Engineering, ITMO University, St. Petersburg, Russia

Abstract In this paper, we theoretically and experimentally prove the possibility of the passive electromagnetic decoupling for two parallel resonant dipoles by a split-loop resonator having the resonance band overlapping with that of the active dipoles. We show that the replacement of the decoupling dipole suggested in the literature as a tool for decoupling of two closely located dipole antennas by our split-loop resonator results in the twofold enlargement of the operation band.

1. Introduction

In many radio-frequency applications, antenna arrays consist of closely located dipoles and their decoupling is required. When the straightforward methods of decoupling (screens or absorbing sheets) are not applicable, one often uses adaptive technique when the decoupling is achieved involving active circuitry—operational amplifiers. However, in multi-input multi-output systems and antenna arrays for magnetic resonance imaging (MRI) the passive decoupling is preferred (Avdievich et al., 2016; Georget et al., 2016; Hurshkainen et al., 2016; H. Li, 2012; Q. Li, 2012; Wang et al., 2015). The keenest situation corresponds to compact arrays when the distance d between two parallel dipole antennas is significantly smaller than $\lambda/10$, where λ is the wavelength in the operation band (it may be, e.g., in the dipole arrays for MRI; Georget et al., 2016; Hurshkainen et al., 2016; Padormo et al., 2016). Then, this distance is not sufficient in order to introduce an electromagnetic band-gap structure or to engineer a defect ground state (H. Li, 2012; Q. Li, 2012; Wang et al., 2015). For passive decoupling of the loop antennas used in MRI radio-frequency coils, one found specific technical solutions working for densely packed arrays (see, e.g., in Avdievich et al., 2016). As to dipole arrays, the passive decoupling is realized either involving the strongly miniaturized (and challenging in its tuning) electromagnetic band-gap structures (Hurshkainen et al., 2016) or arrays of passive scatterers (Georget et al., 2016). However, in both these cases the success was achieved when $d \approx \lambda/12$, whereas in the ultrahigh field MRI there is a need in $d \leq \lambda/30$ (Padormo et al., 2016).

A passive electromagnetic decoupling of two dipole antennas 1 and 2 separated by an arbitrary gap d has been proposed in Lau and Andersen (2012). In this work it was analytically shown that the ideal decoupling (coupling coefficient $S_{12} = 0$) can be achieved placing a similar dipole 3 loaded by a lumped impedance Z_l in the middle between the active dipoles. If these active dipoles are resonant, the ideal decoupling is achieved for $d = 0.1\lambda$ when $\mathrm{Im}(Z_l) = 0$ and $\mathrm{Re}(Z_l) \approx -2\ \Omega$, that is, the decoupling scatterer must be active (see Figure 3 of Lau & Andersen, 2012). If scatterer 3 is shortcut ($Z_l = 0$) the decoupling condition for resonant dipoles cannot be satisfied exactly. However, since the absolute value of the needed negative resistance is as small as $2\ \Omega$, the shortcut dipole also decreases S_{12}, though not up to zero. It is important to stress that this approximate decoupling keeps true, that is, the decrease of S_{12} in the resonance band holds for arbitrary currents and voltages in the feeding points of dipoles 1 and 2. In this Letter we prove that a passive split loop placed in the gap between two active resonant dipoles also results in their true though approximate decoupling within the resonance band. Moreover, this decoupling is more beneficial than that granted by a passive (shortcut) resonant dipole—the operation bandwidth enlarges nearly twice due to the replacement of a dipole by a split loop.

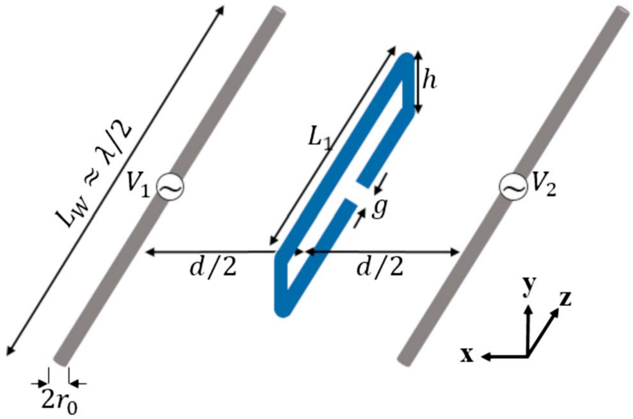

Figure 1. A resonant split-loop resonator 3 located in the middle between antennas 1 and 2.

2. Theory of Decoupling by a Split-Loop Resonator

Now let us prove that decoupling of resonant dipoles 1 and 2 located in free space is possible with a split-loop resonator (SLR) symmetrically located between them. Since the loop contour C comprises the gap g we may consider the SLR as a wire scatterer. The method of induced Electromotive forces (EMFs) is applicable to our SLR, as well as it was applicable to the dipole of Lau and Andersen (2012). Repeating the steps of the derivation presented in Lau and Andersen (2012) it is easy to show that the condition of the ideal decoupling expressed by formula (6) of Lau and Andersen (2012) for the special case when the active dipoles 1 and 3 are decoupled by the similar dipole 2: $Z_l = Z_{13}{}^2 - Z_0 Z_{12}$ (where $Z_0 = Z_{11} = Z_{22} = Z_{33}$ is the self-impedance of all three dipoles) keeps the same form in the case when the decoupling scatterer with the impedance Z_0 is different from these dipoles. Neglecting in this equation Z_l whose absolute value is much smaller than $|Z_{13}|$ and $|Z_{12}|$, we come to the condition of the approximate (but true) decoupling:

$$Z_{13}{}^2 = Z Z_M, \tag{1}$$

that should be implemented for the structure depicted in Figure 1. Here $Z_M = Z_{12}$ is mutual impedance between dipoles 1 and 2, Z is the self-impedance of our SLR, and $Z_{13} = Z_{23}$ is its mutual impedance with antenna 1 or antenna 2. Both Z and Z_M are referred to the scatterer center—reference section located on the solid (top) side of the loop as shown in Figure 2.

In Figure 2 we depict the side view of our structure. A primary source V_1 in the center of dipole 1 induces in our SLR 3 two current modes—an electric one I_e symmetric and an antisymmetric magnetic one I_m with respect to the plane $y = 0$. If the current in the reference section of the SLR, that is, at point $(y = +h/2,\ z = 0)$ is denoted as I_0, both modes have the same amplitude $I_0/2$ at this point, whereas they mutually cancel each other at the gap that can be approximated by point $(z = 0, y = -h/2)$. The distribution of the electric dipole mode along the SLR is similar to that in a straight wire and, therefore, can be approximated as (see, e.g., in Balanis, 2016)

$$f_e(z) \equiv \frac{I_e(z)}{I_0/2} = \frac{\sin k\left(\frac{L_l}{2} - |z|\right)}{\sin \frac{kL_l}{2}}. \tag{2}$$

Contrary to the electric mode, the magnetic one is maximal at the vertical sides of the loop. This is so because these sides are shortcuts if our SLR is considered as a two-wire line. This model of the loop results in the following approximation:

$$f_m(z) \equiv \frac{I_m(z)}{I_0/2} = \pm\frac{\cos k\left(\frac{L_l}{2} - |z|\right)}{\cos \frac{kL_l}{2}}. \tag{3}$$

Sign plus corresponds to the top side of the loop $(y = +h/2)$, sign minus corresponds to the bottom side $(y = -h/2)$.

Let us calculate the mutual impedance Z_{13} between dipole 1 and SLR 3 applying the general formula of the induced EMF method:

$$Z_{13} = \frac{1}{I_1}\int_C E_{13}(l) f_3(l)\, dl, \tag{4}$$

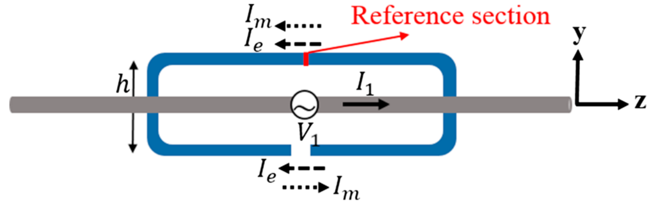

Figure 2. The side view of the structure comprising an active dipole 1 driven by an external voltage V_1 and the passive split-loop resonator 3. Current I_3 induced in the split-loop resonator is the sum of the electric I_e and magnetic I_m modes. At $(y = +h/2,\ z = 0)$ $I_m = I_e = I_0/2$, at $(y = -h/2,\ z = 0)$ $I_m = -I_e = -I_0/2$.

where I_1 is the current at the center of dipole 1, $E_{13}(l)$ is the tangential component of the electric field produced by this primary current at a point l of the wire contour C of scatterer 3, and $f_3(l) = f_e(l) + f_m(l)$ is the current distribution in scatterer 3. Decomposition of the current induced in 3 onto the electric and magnetic modes allows us to split the right-hand side of (4) into electric and magnetic mutual impedances formed by the coupling of the primary current I_1 with the electric and magnetic modes, respectively. The antisymmetry of the magnetic mode results in two mutually canceling EMFs induced in the top ($y = +h/2$) and bottom ($y = -h/2$) sides. In the vertical sides $E_{13} = 0$. Meanwhile, the equivalent EMFs corresponding to the electric mode sum up and (4) is simplified to

$$Z_{13} = \frac{2}{I_1} \int_{-L_l/2}^{L_l/2} E_{13}\left(z, y = \frac{h}{2}\right) f_e(z)\, dz. \tag{5}$$

This formula describes the mutual impedance of two effective dipoles, one of which is dipole 1 length L_w, and the other one is one half of the SLR, for example, its top side L_1. The problem of Z_{13} yields to the symmetric mutual coupling of two parallel dipoles of different lengths. We use the integral formula of King et al. (2002) which allows us to rewrite (5) as

$$Z_{13} = \frac{\eta}{2\pi} \int_{-L_l/2}^{L_l/2} f_e(z) \frac{\sin k\left(\frac{L_l}{2} - |z|\right)}{\sin \frac{kL_l}{2}} F(z, \delta)\, dz. \tag{6}$$

Here $\eta = 120\pi\ \Omega$ is free space impedance and it is denoted

$$F(z, \delta) = \frac{e^{-jkr_+}}{r_+} + \frac{e^{-jkr_-}}{r_-} - 2\cos\frac{kL_w}{2}\frac{e^{-jkr}}{r},$$

$r = \sqrt{z^2 + \delta^2}$, $\delta = \sqrt{(h/2)^2 + (d/2)^2}$, and values r_+ and r_- are distances from two ends of dipole 1 to the integration point:

$$r_- = \sqrt{\left(\frac{L_w}{2} - z\right)^2 + \delta^2}, \quad r_+ = \sqrt{\left(\frac{L_w}{2} + z\right)^2 + \delta^2}.$$

The result of the integration in (6) can be presented in the closed form even in the present case $L_l \neq L_w$ (see, e.g., in Elliot, 1981). However, we will obtain a simpler expression for Z_{13} suitable for our purpose.

Namely, let us assume that both dipole 1 and SLR 3 resonate at the same frequency and the decoupling holds in their resonance band. The resonance of dipole 1 holds when $L_w \approx 0.496\lambda$ and in our SLR the loop inductance resonates with its capacitance. Assuming the capacitance of the gap g to be negligibly small (i.e., correct if $r_0 \ll g \ll L_l$), we may calculate the inductance of our rectangular loop using formulas of Kalantarov and Tseitlin (1986) and its capacitance using formulas of Yossel et al. (1981). Choosing as an example $L_w = 500$ mm and $r_0 = 1$ mm (then the resonance band of dipoles 1 and 2 centered by the resonance frequency can be specified as 290–310 MHz), we fit the resonance band of the SLR to that of the dipoles when $h = 10$ mm and $L_l = 290$ mm.

Since in this case L_l is noticeably smaller than $\lambda/2$, the sinusoidal current distribution (2) can be replaced by its quadratic approximation $f_e(z) = 1 - \left(2z/L_l\right)^2$. This formula seems to be rough, but it is even more accurate (at least when $L_l < \lambda/3$) than the commonly adopted sinusoidal approximation (2) which is not smooth at $z = 0$. Substitution of the quadratic approximation into (6) and variable exchanges $L_l/2 \pm z \to \xi$ yield the right-hand side of this relation to a linear combination of following integrals:

$$J_1 = \int_{\frac{-L_l}{2}}^{\frac{L_l}{2}} \frac{e^{-jk\sqrt{\xi^2+a^2}}}{\sqrt{\xi^2 + a^2}}\, d\xi,$$

$$J_2 = \int_{\frac{-L_l}{2}}^{\frac{L_l}{2}} \xi \frac{e^{-jk\sqrt{\xi^2+a^2}}}{\sqrt{\xi^2 + a^2}}\, d\xi,$$

and

$$J_3 = \int_{\frac{-L_l}{2}}^{\frac{L_l}{2}} \xi^2 \frac{e^{-jk\sqrt{\xi^2+a^2}}}{\sqrt{\xi^2+a^2}} \, d\xi,$$

where a is a constant independent on ξ. Integrals of types J_{1-3} were calculated using the simplest variant of the stationary phase formula (see, e.g., in Bleistein & Handelsman, 1975). In all these integrals the stationary phase point centers the integration interval, whereas the contributions of the ends of this interval (points $\xi = \pm L_l/2$) cancel out in the final expression. This is not surprising because the dipole mode current nullifies at the edges of the SLR.

The stationary phase method is adequate because L_w is large enough and function $F(z)$ is oscillating. Skipping all involved but very simple algebra, the result takes form:

$$Z_{13} \approx \frac{\eta L_l}{3\pi} \left[\frac{kL_w e^{-jk\delta}}{4\sqrt{2\pi\delta}} - \cos\frac{kL_w}{2} \frac{kL_w e^{-jk\Delta}}{2\sqrt{2\pi\Delta}} \right]. \tag{7}$$

Here it is denoted $\Delta = \sqrt{(L_w/2)^2 + \delta^2}$. Further simplification results from the resonant length of our dipoles $kL_w = \pi$. The term with Δ in (7) vanishes and we obtain

$$Z_{13} \approx \frac{\eta L_l e^{-jk\delta}}{24\sqrt{2\pi\delta}}. \tag{8}$$

Now let us calculate the input impedance Z of an individual SLR entering (1). At frequencies near the resonance where the reactance is negligibly small, the input impedance is equal (neglecting the Ohmic losses) to the radiation resistance R_{SLR}. This radiation resistance is a simple sum of R_{el}—that of a Hertzian dipole with effective length L_{eff} (see, e.g., in Balanis, 2016)

$$R_{\mathrm{el}} = \frac{\eta}{6\pi}(kL_{\mathrm{eff}})^2 \tag{9}$$

and R_{mag}—that of a magnetic dipole with effective area S_{eff} (see, e.g., in Balanis, 2016)

$$R_{\mathrm{mag}} = \frac{8\pi\eta}{3}(k^2 S_{\mathrm{eff}})^2. \tag{10}$$

Parameter L_{eff} characterizes the distribution of the electric mode and S_{eff} (magnetic mode) are easily found via simple integration of f_e and f_m that gives in our example case $L_{\mathrm{eff}} \approx L_l$ and $S_{\mathrm{eff}} \approx L_l h$. Then, (9) and (10) for our example case give the radiation resistance of the resonant SLR $R_{SLR} = R_{\mathrm{el}} + R_{\mathrm{mag}} =\approx 70\Omega$. The resonant impedance of a half-wave dipole is also nearly equal R_0 =70 Ω (Balanis, 2016). Therefore, it is reasonable to assume that the input impedance Z of an individual SLR at frequencies near its resonance is practically equal to that of the resonant dipole and can be approximated as $Z \approx R_0(1 + \beta\gamma)$, where $\beta \approx 59$ and $\gamma = (\omega - \omega_0)/\omega_0$ is relative detuning (Kazempour & Begaud, 2001). Substituting this approximation for Z, (8) for Z_{13} and $Z_M \approx (\eta/24\pi kd)\exp(-jkd)$ for two resonant half-lambda dipoles (McConnell, 1989) into (1), we obtain the decoupling condition as

$$\frac{R_0\eta}{24\pi kd} e^{-jkd}(1 + \beta\gamma) = \left(\frac{\eta L_l}{24}\right)^2 \frac{e^{-2jk\delta}}{2\pi\delta^2}. \tag{11}$$

In the case $h \ll d$ $\delta \approx d/2$ and complex exponentials cancel out that reduces (11) to the simplest equation from which we find the detuning γ corresponding to the decoupling

$$\beta\gamma = \left(\eta k L_l^2/dR_0\right) - 1. \tag{12}$$

For $d = 30$ mm (in this case $h = d/3$) and $L_l = 290$ mm, (12) yields $\gamma \approx 0.0423$ that implies the decoupling at the upper edge of the resonance band—at 312.8 MHz. Meanwhile, using a passive resonant dipole we have obtained $\gamma \approx 0.007$, that is, the decoupling holds at 302.8 MHz. In both cases the decoupling holds in the resonance band of the active dipoles.

Table 1
Values of Parameters Used in Simulation and Experiment

Parameter	r_0	L_1	L_w	h	g
Value (mm)	1	290.2	500	7	30

3. Validation of the Theory and Discussion

Numerical investigations of S_{12} parameter are calculated using CST Studio for dipoles 1 and 2 performed of a copper strip printed on FR4 substrate (with the width of 5 mm and the length of 500 mm). Each dipole is split in its center and a lumped port is inserted in the gap and simulated in the absence and presence of ideal matching circuits tuned at the frequency of decoupling. Simulations were done in the absence of our SLR (reference structure) and in its presence. For the reference case, simulation shows that the resonance holds at exactly 300 MHz and S_{12} for the mismatched and matched cases is equal −6 and −4 dB, respectively. In our simulations for the matched case we used the virtual matching circuitry with schematic toolbox of CST Microwave Studio. Namely, for $d = 30$ mm the decoupling at frequency 312.8 MHz is achieved with the values tabulated in Table 1 for the antennas and SLR:

Also, in these simulations we took $g = 30$ mm that is not specified by the theory but satisfies its assumption $r_0 \ll g \ll L_l$.

Numerical result of transmission/reception of the antennas in the mismatched and matched cases are shown in Figures 3 and 4, respectively. After adding the SLR, the decoupling frequency was taken exactly equal to that predicted by our theory (312.8 MHz) and the geometric parameters offering the decoupling at these frequency turned out to be surprisingly close to those predicted by our theory.

Alongside with the transmission/reception response of the structure, we calculated the radiation efficiency and the system radiation pattern in the reference case and in the case when the decoupling SLR is present. In these calculations, one dipole antenna is active and the second one is loaded by 50 Ω resistance (any impedance connected to the centers of two antennas keeps their decoupling condition satisfied). The radiation efficiencies of the active dipole in the reference and decoupled structures are equal (−0.26) and (−2.29) dB, respectively. The difference (−2) dB is expected because the mutual resistance of two parallel dipoles is negative and in the decoupled structure one more scatterer with a dipole mode induced in it by the active dipole is located at the smaller distance from the latter. Figure 5 shows the radiation patterns of the reference and the decoupled structures. Here we follow to the similar calculations in the work of Lau and Andersen (2012) and our dipole array is located in the *XZ* plane, dipoles are oriented along *Z*, and the coordinate frame on the insets corresponds to the polar Θ and azimuthal Φ angles. As shown in Figure 5a, there is no radiation along *Z* in the reference case, the pattern is symmetric in the *YZ* plane, and the pattern is asymmetric in *XY* and *XZ* planes with dominating radiation in the direction from the passive to the active dipole. The same features were noticed in Lau and Andersen (2012), though in this work the dipoles were shorter than $\lambda/2$. However, for the decoupled structure, the difference from Lau and Andersen (2012) is drastic. In our case, the radiation becomes nonzero in any direction and asymmetric in all these planes. There are two important points in this pattern. First, the radiation structure is minimal in the direction from the active dipole to the passive one (see the pattern for $\Phi = 90°$). This is the indication of the low excitation of the passive dipole, in the decoupled structure it is excited only by the passive scatterer. Second, the radiation is nonzero along *Z* because the induced magnetic I_m and electric I_e modes in the SLR are equal, that is, the strong magnetic moment in it is induced that is oriented along *X*. However, because the width of the SLR is small ($h = 7$ mm), the magnetic moment in spite of large I_m is rather small, and the radiation along *Z* direction is comparatively low. In general, the radiation of the decoupled system becomes more isotropic that can be considered as an advantage for some applications.

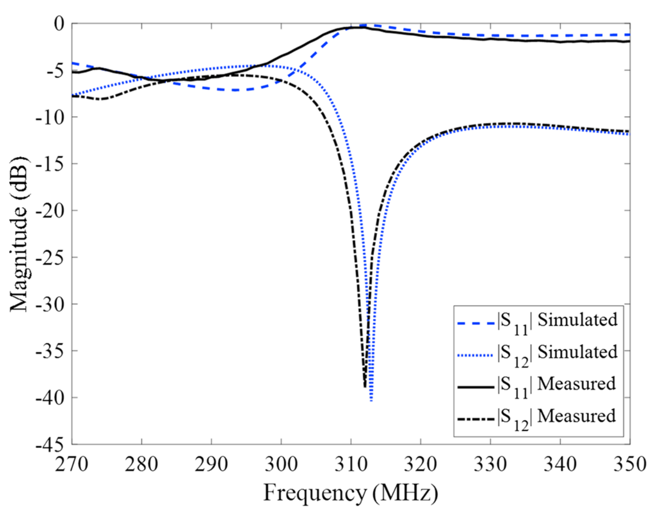

Figure 3. Frequency dependencies of S_{11} and S_{12} for the system of our dipoles 1 and 2 decoupled by our split-loop resonator 3 for the mismatched case.

For further validation of the theory, we built an experimental setup as pictured in Figure 6. In our experiment, a vector network analyzer was

10.1029/2018RS006679

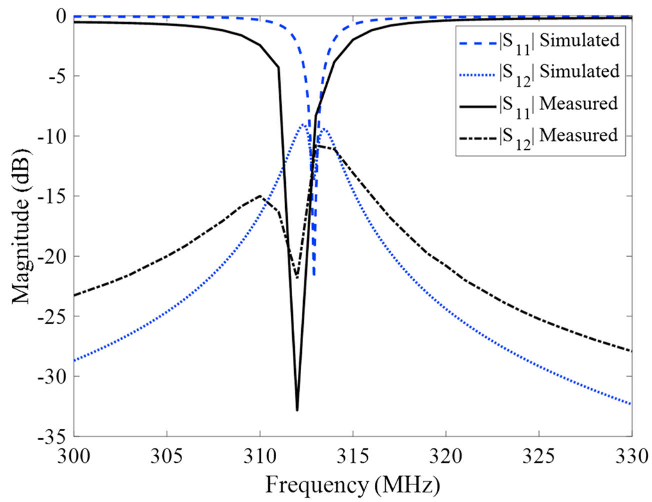

Figure 4. Frequency dependencies of S_{11} and S_{12} for the system of our dipoles 1 and 2 decoupled by our split-loop resonator 3 for the matched case.

connected to our dipole antennas. After calibration, the SLR was inserted between dipole antennas and the S-parameters of the pair of antennas were measured. All parameters of the dipoles and SLR are the same as in the simulations. Our experimental results are presented in Figures 3 and 4. We have avoided building a physical matching circuit for the experimental setup. Instead, we uploaded the measured data into the schematic box of CST Microwave Studio and used the same virtual matching circuitry as we have used in the simulations. In both mismatched and matched regimes, minimum of S_{12} was obtained at 312.8 MHz. Since in the matched and mismatched regimes the ratios of currents (and voltages) in antennas 1 and 2 are different, the coincidence of the frequencies of decoupling for these two regimes is a convincing indication of the true decoupling. As it is seen in Figures 3 and 4, our measurements agree very well with simulations and can be considered as a confirmation of the theory. Decoupling bandwidth of the fabricated structure is enhanced compared to the simulated model most probably due to the influence of the support. We employed a foam desk encapsulated into the paper to fix the experimental setup as shown in Figure 6. Moreover, this support was placed over the wooden table desk. The effective permittivity of such the substrate at ultrashort waves is definitely larger than unity. It should result in higher radiation resistance and distortion of the pattern to the side of the substrate. Higher radiation resistance obviously broadens the resonance band and consequently the band of decoupling broadens, too. In addition, this substrate permittivity manifests in a slight red-shift of the resonance frequency compared to that obtained in simulations.

Our simulations and measurements for the matched case show that the insertion of SLR 3 decreases S_{12} at 312.8 MHz from −4 dB corresponding to the reference structure to −14 dB. The operational band of the

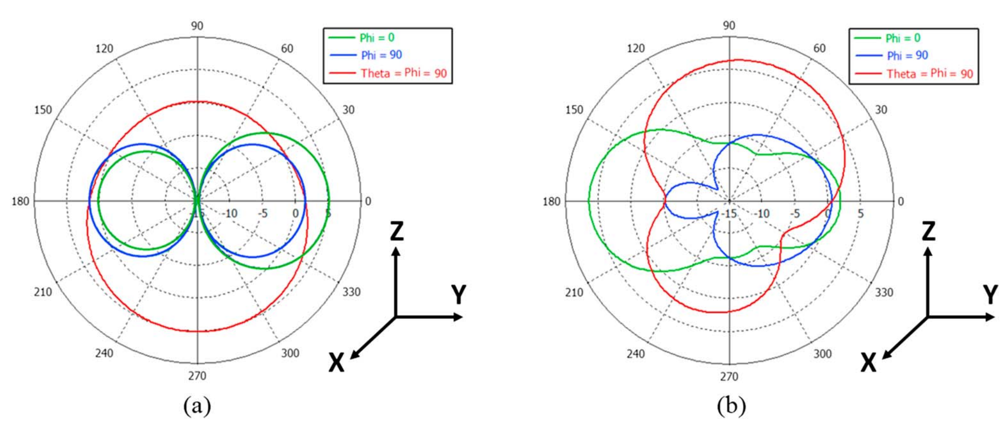

Figure 5. (a) Radiation pattern of the reference case, (b) radiation pattern of the decoupled structure by adding the split-loop resonator.

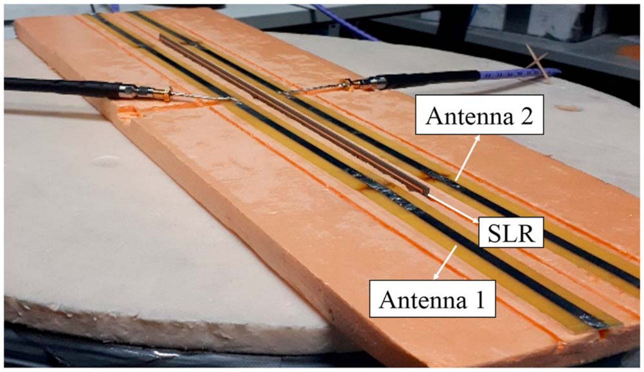

Figure 6. Picture of the fabricated prototype for measurement verification. SLR = split-loop resonator.

decoupled system can be defined as the minimal one of two bands—that of the matching (the band where $S_{11} \leq -15$ dB using a lossless matching circuit) and that of the decoupling (the band where $S_{12} \leq -10$ dB). In these definitions both bands of the matching and decoupling turned out to be equal to 1.42 MHz. This band is twice wider than that offered by a decoupling dipole in the resonant case and this broadening is our main practical result. Having skipped details (to be published elsewhere), a similar numerical and experimental study was done replacing the SLR by a shortcut dipole (as it was suggested but not done in Lau & Andersen, 2012, where the authors concentrated on the decoupling of nonresonant dipoles). In this case the decrease of S_{12} by 10 dB and matching of dipoles 1 and 2 on the level $S_{11} \leq -15$ dB hold in the band of absolute width 0.6 MHz. The gain granted by the SLR is related with the broader band of the dipole mode compared to the case of the decoupling dipole. Really, the SLR consists of two rather long parallel wires (connected to each other by two short wires of length h). The electric dipole mode (responsible for the decoupling) corresponds to two equal currents in these long wires. Therefore, the dipole mode in the SLR is nearly equivalent to that in a strip of width h. However, our SLR is not fully equivalent to such a strip. Due to the coupling between the electric and magnetic dipole modes it resonates at a frequency where its length is smaller than $\lambda/2$. It is similar to the loading of a rather wide ($h \gg r_0$) metal strip by an inductive load. The resonance band of the loaded strip dipole is wider than that of the half-wave dipole performed of the wire with radius r_0. As a result, the operational bandwidth of the system decoupled by the SLR is wider than that of the system decoupled by a passive dipole.

4. Conclusion

We have theoretically and experimentally proved that the approximate (but true) decoupling of two very closely located resonant dipoles can be granted by a passive scatterer whose geometry is strongly different from the similar dipole suggested in the work of Lau and Andersen (2012). The usefulness of the replacement of the dipole scatterer is the enlarged operation bandwith (from 0.2% to 0.47%). This operation band is sufficient for several practical applications such as transceiver dipole arrays for ultrahigh field MRI (Georget et al., 2016; Hurshkainen et al., 2016; Padormo et al., 2016). Moreover, with this work we have shown that the decoupling of two dipole antennas is possible using a passive scatterer of different type. Earlier, it was proved only for the dipole of the same length. Therefore, our study opens the door to the search of decoupling passive scatterers which could be even better than our SLR.

Acronyms

MRI Magnetic resonance imaging
SLR Split-loop resonator
EMF Electromotive force

Acknowledgments
Theoretical studies were supported by the Russian Science Foundation (Project 18-19-00482). Experiments were supported by the European Union's Horizon 2020 research and innovation program under grant agreement 736937. The data presented were obtained through implementation of the following methods: (1) stationary phase method as described in the paper, (2) CST Studio software, (3) experiment described in the paper, (4) literature data described in the citations. The numerical and experimental data are available upon request from the corresponding author.

References

Avdievich, N. I., Pan, J. W., & Hetherington, H. P. (2016). Resonant inductive decoupling (RID) for transceiver arrays to compensate for both reactive and resistive components of the mutualimpedance. *NMR in Biomedicine*, *26*, 1547–1554.
Balanis, C. A. (2016). *Antenna theory: Analysis and design* (4th ed.).: Wiley.
Bleistein, N., & Handelsman, R. (1975). *Asymptotic expansions of integrals* (Vol. 36). New York, NY: Dover.
Elliot, R. S. (1981). *Antenna theory and design*, vol. 225. Englewood Cliffs, NJ: Prentice Hall.
Georget, E., Luong, M., Vignaud, A., Giacomini, E., Chazel, E., Ferrand, G., et al. (2016). Stacked magnetic resonators for MRI RF coils decoupling. *Journal of Magnetic Resonance*, *175*, 11–18.
Hurshkainen, A. A., Derzhavskaya, T. A., Glybovski, S. B., Voogt, I. J., Melchakova, I. V., Van den Berg, C. A. T., & Raaijmakers, A. J. E. (2016). Element decoupling of 7 T dipole body arrays by EBG metasurface structures: Experimental verification. *Journal of Magnetic Resonance*, *269*, 87–96.
Kalantarov, P. L., & Tseitlin, A. A. (1986). Calculation of inductance. *Energoatomizdat*, *187*.
Kazempour, A., & Begaud, X. (2001). Numerical and analytical model of standard antennas for 30 MHz to 2 GHz. *IEEE EMC International Symposium. Symposium Record. International Symposium on Electromagnetic Compatibility* (pp. 620–625). Montreal, Que., Canada.
King, R. W. P., Fikioris, G. J., & Mack, R. B. (2002). *Cylindrical antennas and arrays*, vol. 160. Cambridge: Cambridge University Press.
Lau, B. K., & Andersen, J. B. (2012). Simple and efficient decoupling of compact arrays with parasitic scatterers. *IEEE Transactions on Antennas and Propagation*, *60*, 464–472.
Li, H. (2012). Decoupling and evaluation of multiple antenna systems in compact MIMO terminals (Ph.D. dissertation, Dept. Elect. Eng.), KTH Univ., Stokholm, Sweden.

Li, Q. (2012). Miniaturized DGS and EBG structures for decoupling multiple antennas on compact wireless terminals (Ph.D. dissertation, Dept. Elect. Eng.), Loughborough Univ., Loughborough, UK.
McConnell, R. A. (1989). The effect of dipole coupled impedances on calibration. *National Symposium on Electromagnetic Compatibility* (pp. 16–18). Denver, CO.
Padormo, F., Beqiri, A., Hajnal, J. V., & Malik, S. J. (2016). Parallel transmission for ultrahigh-field imaging. *NMR in Biomedicine*, *29*, 1145–1161.
Wang, S. M., Hwang, L. T., Lee, C. J., Hsu, C. Y., & Chang, F. S (2015). MIMO antenna design with built-in decoupling mechanism for WLAN dual-band applications. *Electronics Letters*, *51*, 966–968.
Yossel, Y. Y., Kachanov, E. S., & MStrunski, M. G. (1981). Calculation of electric capacitance. *Energoizdat*, *212*.